Journal of Rock Mechanics and Geotechnical Engineering 8 (2016) 660–671

Contents lists available at ScienceDirect

Journal of Rock Mechanics and Geotechnical Engineering

journal homepage: www.rockgeotech.org

Full length article

Influence of fault slip on mining-induced pressure and optimization of roadway support design in fault-influenced zone

Hongwei Wang [a,b,*], Yaodong Jiang [a,b], Sheng Xue [c], Lingtao Mao [d], Zhinan Lin [a], Daixin Deng [a], Dengqiang Zhang [a]

[a] School of Mechanics and Civil Engineering, China University of Mining & Technology, Beijing, 100083, China
[b] State Key Laboratory for GeoMechanics and Deep Underground Engineering, China University of Mining & Technology, Beijing, 100083, China
[c] CSIRO Energy, PO Box 883, Kenmore, QLD, 4069, Australia
[d] State Key Laboratory of Coal Resources and Safe Mining, China University of Mining & Technology, Beijing, 100083, China

ARTICLE INFO

Article history:
Received 1 January 2016
Received in revised form
15 March 2016
Accepted 17 March 2016
Available online 25 June 2016

Keywords:
Physical modeling
Fault slip
Mining-induced pressure
Roadway support design
Field observation

ABSTRACT

This paper presents an investigation on the characteristics of overlying strata collapse and mining-induced pressure in fault-influenced zone by employing the physical modeling in consideration of fault structure. The precursory information of fault slip during the underground mining activities is studied as well. Based on the physical modeling, the optimization of roadway support design and the field verification in fault-influenced zone are conducted. Physical modeling results show that, due to the combined effect of mining activities and fault slip, the mining-induced pressure and the extent of damaged rock masses in the fault-influenced zone are greater than those in the uninfluenced zone. The sharp increase and the succeeding stabilization of stress or steady increase in displacement can be identified as the precursory information of fault slip. Considering the larger mining-induced pressure in the fault-influenced zone, the new support design utilizing cables is proposed. The optimization of roadway support design suggests that the cables can be anchored in the stable surrounding rocks and can effectively mobilize the load bearing capacity of the stable surrounding rocks. The field observation indicates that the roadway is in good condition with the optimized roadway support design.

1. Introduction

Fault is a tectonic fracture in the Earth's crust along which slippage has taken place (Bryant, 2013). It can be classified as normal, reverse and strike-slip types according to the direction in which the relative movement of hanging wall and footwall has taken place. Due to the significant stress redistribution, irregular deformation of rock masses and a large amount of elastic energy accumulated around reverse fault plane, most major catastrophic fault slip had occurred around the world (Castro et al., 2009; Orlic and Wassing, 2013; Jiang et al., 2014). The fault slip mainly refers to a sudden and intense fault slip induced by extraction of longwall panel in coal mining industry, which could cause significant damage to mine openings where men and machinery are present. Therefore, prediction and prevention of fault slip have been major safety concerns for long-term mine safety and productivity in underground coal mines.

Numerous studies have been conducted to obtain a comprehensive understanding of fault slip. Firstly, the prediction and prevention of fault slip must take into account the fault geometry and associated structures. The imaging and mapping of fault structure therefore play a significant role in investigating fault slip. Based on this idea, a high-resolution seismic reflection technique was used by Gochioco and Cotten (1989) to locate faults in coal mines. In their work, several faults were detected and interpreted from the seismic section and the displacement of faults was estimated additionally to design a safer and more productive coal mine in the faulted zone. Kecojevic et al. (2005) presented a computer mapping for multiple coal seams and multiple reverse faults in Columbia using MineScapek geological modeling software, and pointed out that the effective mapping of faults in coal mining is critical for reasons of economics and safety. In order to obtain a three-dimensional (3D) and visual fault model, Scheidhauer et al.

* Corresponding author. Tel.: +86 10 62335261.
E-mail address: whw@cumtb.edu.cn (H. Wang).
Peer review under responsibility of Institute of Rock and Soil Mechanics, Chinese Academy of Sciences.

http://dx.doi.org/10.1016/j.jrmge.2016.03.005

(2005) developed an efficient 3D high-resolution seismic reflection system in Switzerland. Furthermore, Peng et al. (2008) and Du et al. (2015) developed a 3D seismic integrated interpretation system to investigate the distribution of primary fault structure in Guqiao coal mine in China. Similarly, Hlousek et al. (2015) presented an investigation of a 3D seismic survey acquired near Schneeberg in the western Erzgebirge.

Deep mining conducted under tectonic stress conditions induced by the fault reactivation or fault slip could lead to the occurrence of coal bumps. According to Jiang et al. (2014) and Jiang (2014), occurrence of serious coal bumps in Yima mining district in 2011 in China could be explained as a consequence of the intensive compressive stress imposed during the reactivation process of fault F16. Therefore, many efforts have been made for better understanding of the mechanism of fault reactivation. Based on the large amount of survey data obtained from several coal mines with faults in the US, Wallace and Morris (1986) conducted a review work and pointed out that the fault surface was absolutely not a planar and the irregularities characteristics would constraint the study of the fault slip. Therefore, the characteristic of fault reactivation is significantly correlative with the roughness of fault surface. Recently, Sainoki and Mitri (2014a,b, 2015) conducted a series of researches to simulate the effect of fault slip with various methods. In their works, the influences of mining depth, friction angle, dilation angle and stiffness of fault on the fault slip were investigated. In addition, the fault-surface roughness and slip weakening behavior were also studied to estimate the fault slip intensity by the FLAC^{3D} code. Also, Jain et al. (2013) focused on the fault angles to simulate the fault reactivation phenomenon.

In the past decades, occurrence of coal bumps induced by the fault slip has been increasing due to the increasing mining depth and concentrated tectonic stress. Hence, the collection of precursory information for the fault slip is imperative in the controlling and prevention of coal bumps. According to Jiang et al. (2013), the high-risk fault slip could be determined by the sharp increase of normal and shear stresses monitored in and around the fault plane. Singh et al. (1998), Vishal et al. (2012), and Tripathy and Singh (2016) conducted a series of rock slip tests to obtain the value of critical velocity to study the transformation of the stick slip motion to steady motion. Considering the potential coal bumps risk induced by the coupling effect of fault and coal pillar, Li et al. (2014) pointed out that the occurrence of coal bumps in the fault and pillar areas was induced by the concentration of static stress on the pillar and the dynamic stress induced by fault reactivation. Besides, the monitoring of seismic event was proved to offer significant insights into the fundamental nature of the coal bumps (Cook, 1964; Ortlepp, 2002; McKinnon, 2006; Li et al., 2011; Singh et al., 2012; Jain et al., 2013). The incorporated microseismic and mining-induced pressure prediction system (Jiang et al., 2011; Liu et al., 2014) and distributed microseismic monitoring system (Dou et al., 2012; Cai et al., 2014) are effective for predicting the fault slip over the past decades in China.

As mentioned above, a large number of experimental studies, numerical investigations and field tests have been undertaken for characterizing the fault geometry and associated structures, analyzing the mechanism of fault reactivation and predicting the fault slip induced by mining activities. However, there are few studies on the influence of the multi-fault structure on the mining-induced pressure and obtaining a representative characteristic of deformation of overlying strata under dynamic pressure in the fault-influenced zones to optimize roadway support design. In addition, the studies of characteristic of mining-induced pressure with and without fault influences are also rarely reported. Therefore, in order to further optimize the roadway support design system for the fault-influenced zone, a physical model with two fault structures is established according to the geological conditions of an underground coal mine in Shanxi Province, China. The studies of mining-induced pressure in the uninfluenced and fault-influenced zones are conducted to characterize the overlying strata collapse. An optimization of roadway support design for fault-influenced zones is carried out to maintain the roadway stability and the field tests are conducted to verify the effectiveness of roadway support design.

2. Background of coal mine

2.1. Mining site

The physical model is established according to the geological setting of Zhengli underground coal mine in Shanxi Province, China. In addition, the field test is also conducted in this site. The Zhengli coal mine has an annual production of 1.5 million tons of raw coal. The mining site of Zhengli coal mine is 5 km long along the north-south direction and 3.2 km wide along the east-west direction, covering a total mining area of 9.26 km^2. Fig. 1 presents the mining layout of mining area #1 of Zhengli coal mine. There are four mineable coal seams in this coal mine. The coal seam #4^{-1} is being mined currently with a dip angle of 9° and an average mining height of 3.9 m. The surrounding rocks mainly consist of mudstone, sandy mudstone, fine-grained sandstone, and medium-grained sandstone. The general stratigraphy of this mine is shown in Fig. 2. The mine currently uses the longwall mining method at the depths from 645 m to 720 m below the ground surface.

2.2. Geological setting of main studied area

A major research project undertaken recently by China University of Mining & Technology, Beijing (CUMTB) in collaboration with Zhengli coal mine is to characterize the mining-induced pressure influenced by the fault structure. As shown in Fig. 1, based on the geological conditions of the haulage roadway of longwall panel #14^{-1}103 in mining area #1, the physical model is established and the field test is conducted. Since the mining panel #14^{-1}103 is being mined, the haulage roadway is in service under dynamic pressure. It has an overburden depth of 650 m, and is 1589 m long along the strike direction and 180 m wide along the dip direction. The mining coal seam is about 4 m thick. The geological core log of the surrounding rocks shows that the main roof is fine-grained sandstone with an average thickness of 5.4 m and uniaxial compressive strength of 41 MPa. The panel floor is composed of mudstone and is approximately 3.6 m thick. The roadway is of rectangular shape with a width of 4.5 m and height of 2.8 m. The roof support system in the roadway consists of bolts, cables and steel mesh. Fig. 3 shows the layout of the original support design of haulage roadway for longwall panel #14^{-1}103 with detailed support parameters.

The presence of seven faults (Table 1) has been predicted in mining area #1 before the mining of Zhengli coal mine begins by means of drilling and electromagnetic radiation exploration. Among these faults, faults F36 and F37 located in longwall panel #14^{-1}103 are the major geologic disturbance that greatly interrupt coal seam and severely interfere the mining operation. With the influence of the two faults, several accidents occurred in the process of mining and are summarized as follows: (1) Since the presence of faults could weaken the roof and ribs of roadway, the sudden and severe roof collapse have taken place for many times; (2) Since the dynamic pressure induced by the coupling effect of mining activities and fault reactivation is imposed on the original support system, many bolts have been damaged. Therefore, the influence of fault structure on the mining-induced pressure should be understood and the support design should be specially optimized for the fault-influenced zone.

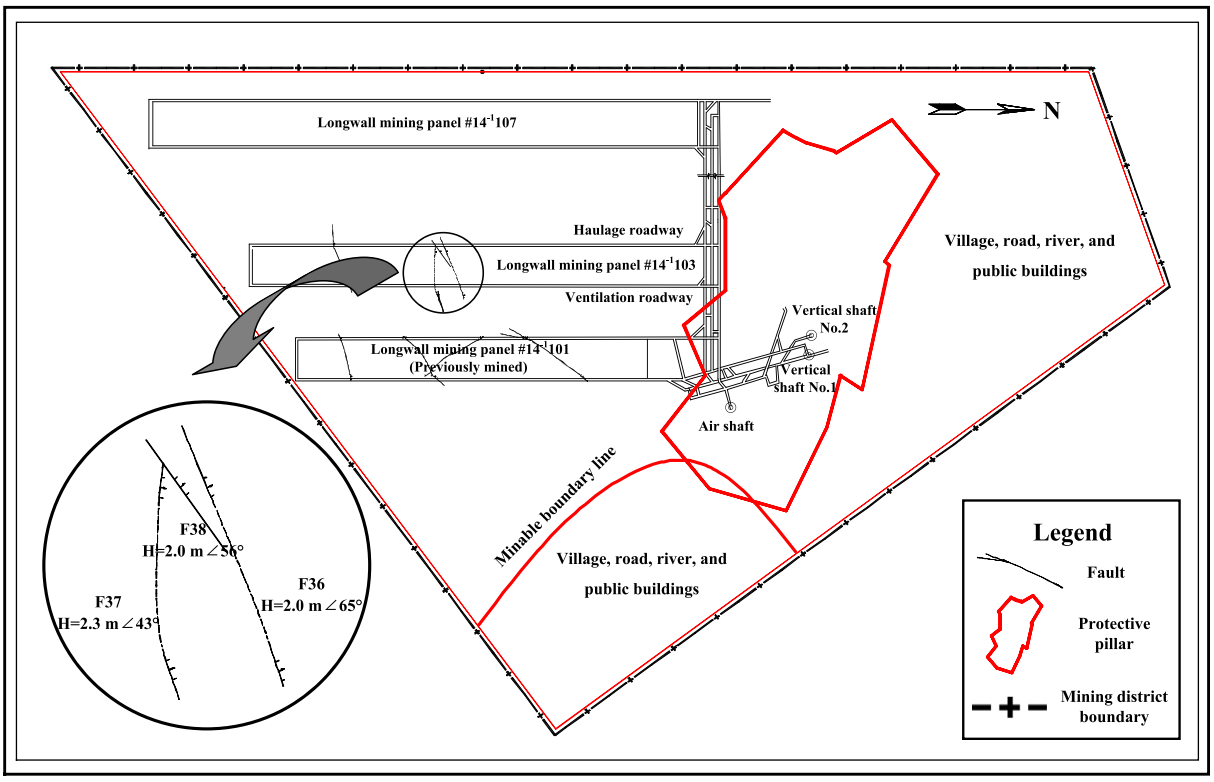

Fig. 1. Mining layout of mining area #1 of Zhengli coal mine.

Stratum No.	Geological legend	Rock type	Thickness (m)	Density (kg/m^3)	Uniaxial compressive strength (MPa)	Young's modulus (GPa)	Poisson's ratio
1		Mudstone	4.7	2647	10.4	10.0	0.35
2		Sandy mudstone	5.2	2740	24.6	16.5	0.30
3		Fine sandstone	5.4	2687	41.0	29.4	0.26
4		Coal seam #4^{-1} Sandy mudstone Coal seam #4^{-1}	3.9	1360	3.0	2.5	0.36
5		Sandy mudstone	3.6	2740	24.6	16.5	0.30
6		Coal seam #4	2.3	1360	3.0	2.5	0.36
7		Fine sandstone	5.9	2687	41.0	29.4	0.26
8		Sandy mudstone	2.3	2740	24.6	16.5	0.30
9		Medium sandstone	4.6	2723	37.3		

Fig. 2. General stratigraphy of coal seams and rock strata.

2.3. Physical and mechanical parameters

According to Wang et al. (2015), the uniaxial compressive strength, Young's modulus, Poisson's ratio, cohesion and internal friction angle of rocks are required to analyze the mechanical behaviors of the rock masses in this study. Therefore, the key physical and mechanical properties of the surrounding rocks are determined by laboratory testing on samples obtained from exploration drilling cores and rock blocks taken from Zhengli coal mine. The uniaxial compression tests are undertaken to determine the uniaxial compressive strength, Young's modulus and Poisson's ratio. These testing results, the panel stratigraphy, and other key geotechnical parameters of the coal seam, roof and floor strata are shown in Fig. 2.

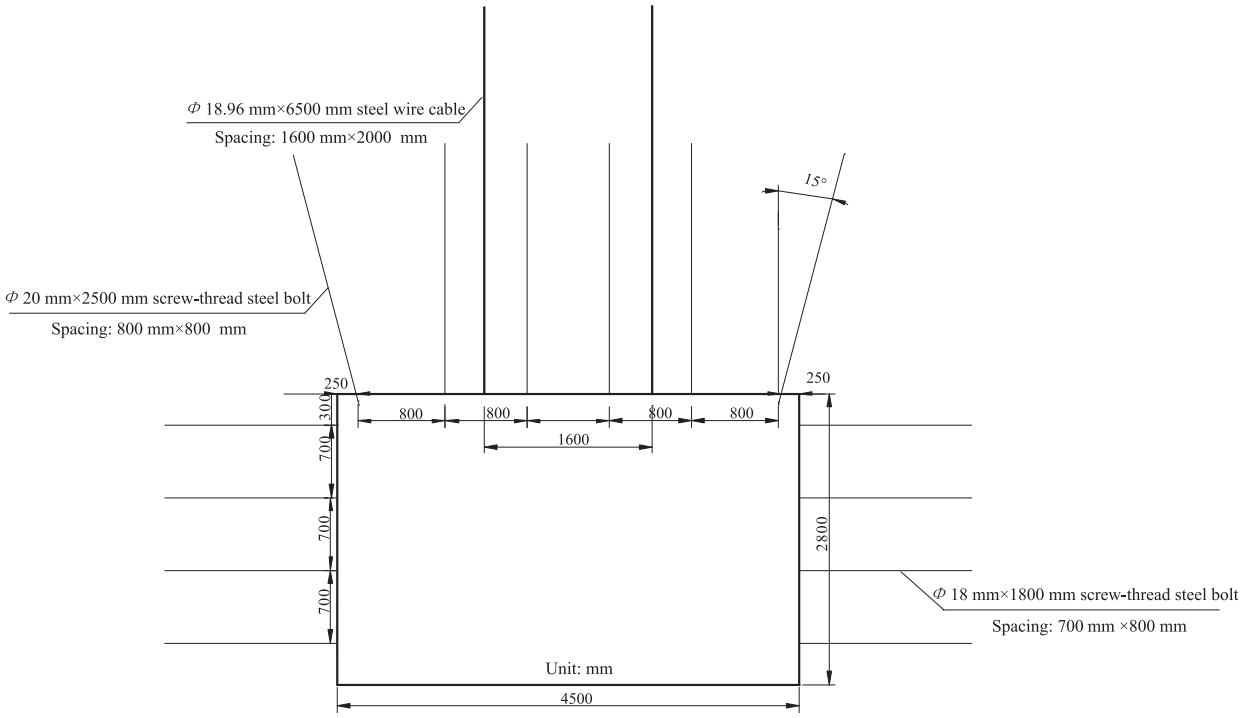

Fig. 3. Layout of the original support design of haulage roadway of longwall panel #14^{-1}103.

Table 1
Parameters of seven faults in mining area #1 of Zhengli coal mine.

Fault	Location	Strike direction (°)	Dip direction (°)	Dip angle (°)	Fault throw (m)
F34	Longwall panel #14^{-1}101	265	175	50	1
F36	Longwall panel #14^{-1}103	250	340	65	2
F37	Longwall panel #14^{-1}103	250	340	43	2.3
F35	Longwall panel #14^{-1}101	140	50	48	0.6
F32	Longwall panel #14^{-1}101	250	340	43	5.5
F38	Longwall panel #14^{-1}103	232	322	56	2
F39	Longwall panel #14^{-1}103	333	243	30	1.5

3. Physical modeling and its procedure

3.1. Brief description of physical modeling

The overlying strata movement behavior induced by the mining activities can be effectively represented by physical modeling. Due to the limitations of field tests and numerical simulations, e.g. long-term monitoring, high cost, and uncertainty regarding the assumptions on the constitutive model and material properties, the physical modeling has been widely utilized by many researchers to study the mining-induced pressure (Ghabraie et al., 2015), thick seam mining (Goyal et al., 1997), ground subsidence in mining engineering (Ghabraie et al., 2015), shallow opening design in jointed rock mass (Fuenkajorn and Phueakphum, 2010), underground carven design (Zhu et al., 2011), dam foundation stability in hydropower engineering (Liu et al., 2003), and fault slip process in geological engineering (Singh and Singh, 1991, 1992a,b; Monjezi and Singh, 2000; Jiang et al., 2013).

Since the physical modeling utilized in the engineering requirements should satisfy the similarity theory, the model geometry, material's strength and density, boundary, and in situ stress state should be analyzed. According to the elasticity and similarity theories (Li, 1988), the prototype and model should simultaneously satisfy the equilibrium differential equation. Therefore, the model geometry, material's strength and density should meet the following equation:

$$\frac{C_\sigma}{C_\rho C_L} = 1 \tag{1}$$

where C_L, C_σ and C_ρ are the similarity coefficients of model geometry, material's strength and density, respectively. These parameters can be calculated by

$$C_L = \frac{L_\mathrm{p}}{L_\mathrm{m}}, C_\rho = \frac{\rho_\mathrm{p}}{\rho_\mathrm{m}}, C_\sigma = \frac{\sigma_\mathrm{p}}{\sigma_\mathrm{m}} \tag{2}$$

where L_p, σ_p and ρ_p represent the prototype's geometry, strength and density, respectively; and L_m, σ_m and ρ_m stand for the model's geometry, strength and density, respectively.

If the coefficients C_ρ and C_L are determined, the coefficient C_σ can be obtained according to Eqs. (1) and (2). It should be noted that these three coefficients are dimensionless parameters.

The materials selected as analogs for the coal seam and overlying strata have components of aggregate material and binder. The aggregate material consisting of fine sand is the main ingredient in the physical model. The plaster and lime powder in the binder can improve the strength and brittleness of material, respectively. Therefore, the proportional complex of sand, plaster and lime powder associated with water can be employed as a certain material to establish the physical model.

3.2. Establishment of physical model

The physical model with a length of 4.2 m, height of 1.5 m and thickness of 0.25 m is established on the two-dimensional platform installed in the mining laboratory in CUMTB, as shown in Fig. 4. Considering the thickness of coal seam and overlying strata

and the dimensional characteristic of platform, the similarity coefficient C_L is set as 200. According to the empirical value of the mass of sand, plaster and lime powder mixture, the similarity coefficient C_ρ should be set as 1.2–1.7 (Jiang et al., 2013). In this study, it is set as 1.5. Hence, the similarity coefficient C_σ can be calculated as 300 from Eq. (1). The proportions of mixture including sand, lime powder and plaster for different rock strata are listed in Table 2. The mica powder is added between each layer of physical model to improve the separation of different layers.

In order to obtain the fault slip during the extraction of longwall panel, boundary conditions should be set around the physical model. The left, right and bottom boundaries of model are rigidly restricted due to the constraint of the platform. At the top of the model, a vertical load is applied to simulate the overburden weight. The advancement direction with the mining step of 5 cm is from left to right of the model. Therefore, to reduce the boundary effects, two pillars with width of 40 cm are remained at left and right boundaries of model, as shown in Fig. 4.

Since it is difficult to simulate the geological evolution and fault formations, the faults F36 and F37 are progressively formed from bottom to top during the establishment of physical model. Fig. 4b presents the schematic diagram of the process of fault construction in the physical model. The mica powder is added as well to the fault plane to improve the fault slip.

Table 2
Proportions of mixture including sand, lime powder and plaster for different rock strata.

Stratum	Proportion of sand, lime and plaster
Mudstone	9:8:2
Sandy mudstone	9:8:2
Fine sandstone	8:6:4
Medium sandstone	8:5:5
Coal seam	9:7:3

3.3. Monitoring scheme

Stress and deformation are monitored in the physical modeling. As shown in Fig. 4a, strain sensors are distributed in the roof 40 cm above the coal seam #4^{-1} to detect stress change during the coal seam mining. There are 13 sensors placed in front of the fault F37. The spacing between sensors is 15 cm. The static strain monitor CM-2B with 32 monitoring channels and minimum monitoring interval of 5 s is used to record the signals transmitted from the strain sensors. The strain change data from sensors are converted to stress change according to the almost linear stress–strain relationship of the strain sensors (Fig. 5).

The digital image correlation (DIC) is applied to observe the deformation of overlying strata during the coal seam mining (Kozicki and Tejchman, 2007; Lin et al., 2010; Mao et al., 2013, 2015). The DIC has the feature of high-speed application to

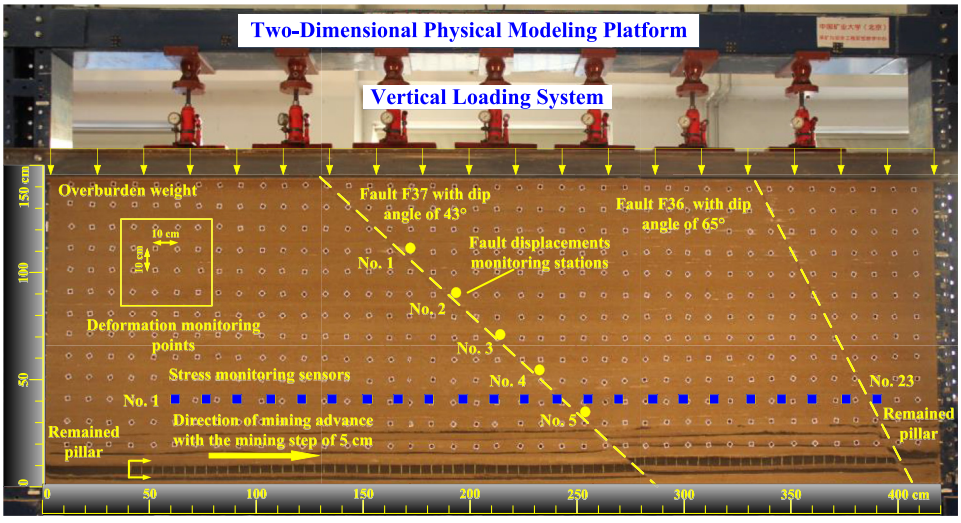

(a) Physical model and monitoring system.

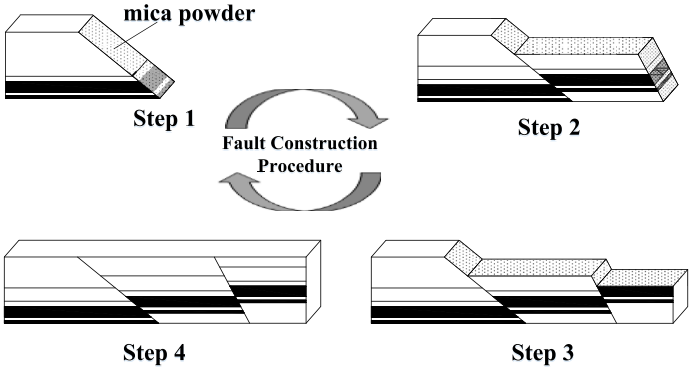

(b) Process of fault construction.

Fig. 4. Schematic diagrams of physical model and faults construction.

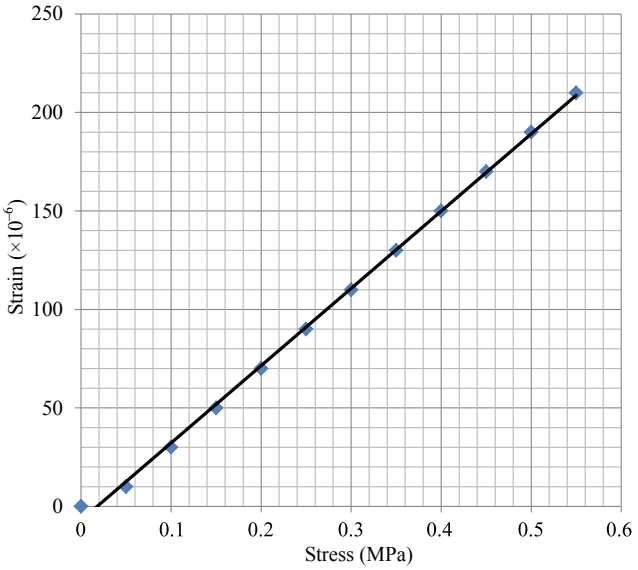

Fig. 5. Stress–strain relationship of the strain sensors.

dynamic measurement, flexible selection of measurement area from 2 mm to 2 m, high measuring sensitivity of 1/100,000 of the field of view, and surface contour, 3D displacement and strain contour can be shown. In this study, the objected points with point-to-point spacing of 10 cm along the horizontal and vertical directions are arranged on the physical model plane, as shown in Fig. 4a.

4. Monitoring results and analyses

This section describes the monitoring results, including the characteristics of overlying strata movement, roof caving process, and distribution of mining-induced pressure and displacement around the fault zones. These results are analyzed to understand the influence of the fault structure on the mining-induced pressure. In this physical modeling, the characteristics of overlying strata movement and mining-induced pressure in the uninfluenced and first fault-influenced zones are focused on. The zones between the first and second faults will be investigated by numerical and physical modeling and be published later.

4.1. Characteristics of overlying strata and faults movement

4.1.1. Characteristics of overlying strata movement

The experimental descriptions and several representative images of overlying strata movement during the coal mining are presented in Table 3 and Fig. 6, respectively. It is noted that the overlying strata have experienced first weighting and 16 times of periodic weighting during the extraction of coal seam. In this process, the uninfluenced and fault-influenced zones can be clearly observed. The roof caving span for the first caving is approximately 45 cm in the experimental scale. The span of roof periodic caving is approximately 15 cm in the uninfluenced zone, and it is nearly 10 cm in the fault-influenced zone. The boundary between the two zones is the key to the optimization of roadway support design, and it will be accurately determined by employing the stress and displacement data in Sections 4.2 and 4.3. The span of periodic roof caving in the zone between the faults F37 and F36 varies from 10 cm to 15 cm, indicating the severe fracture propagation in the roof strata in this region.

Table 3
Experimental descriptions of overlying strata movement.

Advancement of mining face (cm)	Distance to fault (cm)	Description	Span of periodic roof caving (cm)	Influence on faults
5	235	No change		
35	200	Slight roof separation		
40	195	Immediate roof caving		
45	190	The 1st main roof caving	45	
60	175	The 1st periodic main roof caving	15	
75	160	The 2nd periodic main roof caving and overlying strata collapse	15	
90	145	The 3rd periodic main roof caving and severe overlying strata collapse	15	
105	130	The 4th periodic main roof caving	15	
115	120	The 5th periodic main roof caving	15	
120	115			Slight influence
130	105	The 6th periodic main roof caving	10	
140	95	The 7th periodic main roof caving and severe overlying strata collapse	10	
150	85	The 8th periodic main roof caving and severe overlying strata collapse	10	Slight influence
165	70	The 9th periodic main roof caving	10	
175	60	The 10th periodic main roof caving and severe overlying strata collapse	10	Severe influence
185	50	The 11th periodic main roof caving	10	
190	45			Fractures appear around the fault
195	40	The 12th periodic main roof caving	10	
205	30	The 13th periodic main roof caving and slight fault slip	10	Slight fault slip
215	20	Frequent immediate roof caving, the 14th periodic main roof caving, severe overlying strata collapse and severe fault slip	10	Severe fault slip
225	10	The 15th periodic main roof caving	10	
230	5	The 16th periodic main roof caving and fault slip	10	Severe fault slip
235	0			Fault slip

4.1.2. Characteristics of faults movement

Faults movement is the major concern in this paper. According to the experimental results in Table 3 and Fig. 6, the fault F37 starts to make a slight response to the extraction of coal seam when the mining face is advanced to the position 115 cm away from the fault F37. The violent movement of fault F37 occurs when the distance to the fault reaches 20 cm. These data are of significance to better

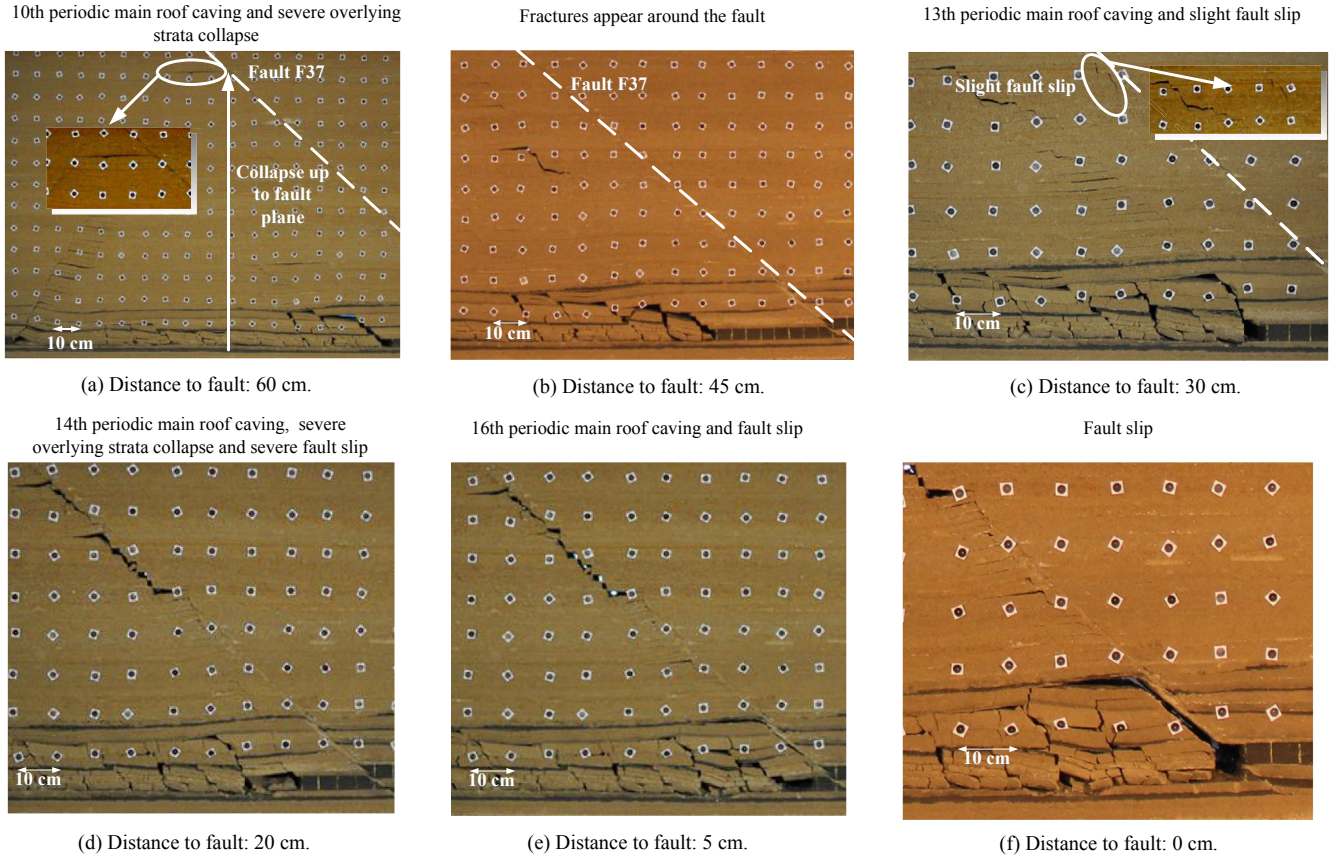

Fig. 6. Representative images of overlying strata movement during coal mining.

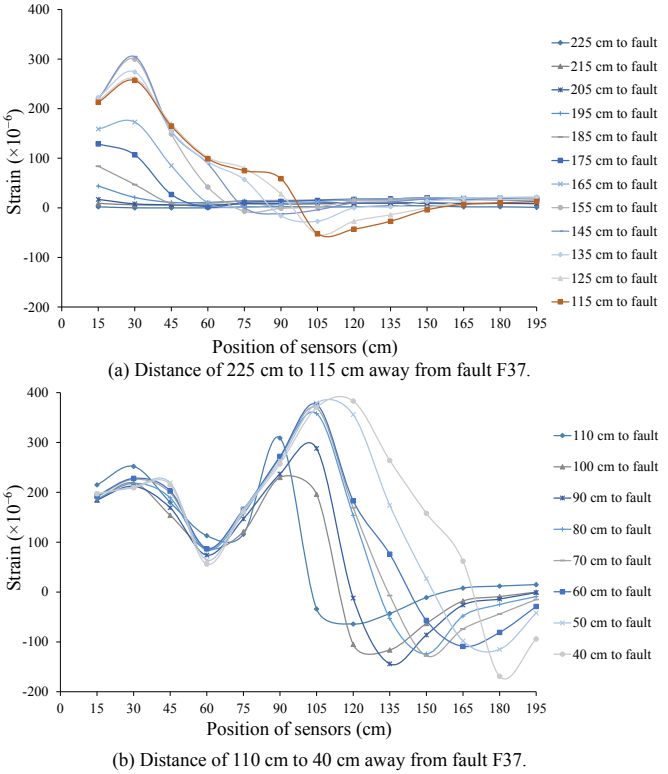

Fig. 7. Strain variation curves detected from sensors Nos. 1–13 during advancement of mining face.

understand the fault reactivation during the coal seam mining, which is incorporated with the stress and displacement results in Sections 4.2 and 4.3 to present the precursory information of mining-induced fault slip.

4.2. Distribution of mining-induced pressure

4.2.1. Determination of the boundary between uninfluenced and fault-influenced zones

To understand the mining-induced pressure in the normal and fault-influenced zones, the boundary between the two zones

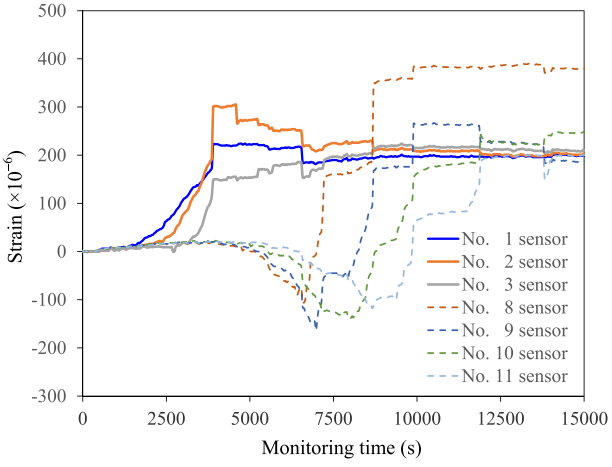

Fig. 8. Distribution of mining-induced pressure during coal seam mining in uninfluenced and fault-influenced zones.

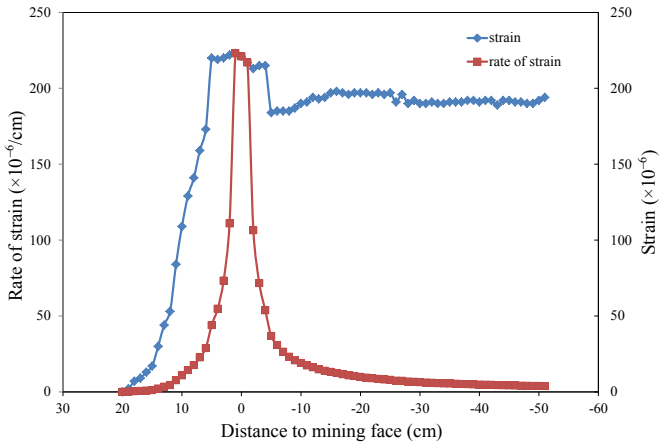

Fig. 9. Distribution of mining-induced pressure for sensor No. 1 with distance to mining face in uninfluenced zone.

should be firstly determined. Since the fault reactivation is induced by the mining activities, the extraction of coal seam is the dominant factor and the characteristics of mining-induced pressure will be different in the normal and fault-influenced zones. Fig. 7 shows a series of strain variation curves detected from sensors Nos. 1–13 during the advancement of mining face. The mining-induced pressure varies significantly when the distance between the mining face and fault F37 reaches 115 cm. In other words, the stress curves show a sharp fluctuation in the fault-influenced zone (Fig. 7b), whereas they are relatively stable in the uninfluenced zone (Fig. 7a). This boundary should be consistent with the start position of mining-induced fault slip which is observed from the experimental phenomena. The boundary between the uninfluenced and fault-influenced zones is therefore determined to be 115 cm away from the fault F37.

4.2.2. Mining-induced pressure in uninfluenced zone

Fig. 8 presents the behavior of mining-induced stress with the monitoring time for sensors Nos. 1–3 in the uninfluenced zone. It can be seen that the stress is relatively low when the mining begins and increases sharply at a certain time in front of the mining face. Fig. 9 shows the behavior of mining-induced stress with the distance to mining face for sensor No. 1. These results suggest that the abutment stress reaches a peak value at a distance of 5 cm in front of the mining face in the experimental scale (10 m in the prototype scale). The length of influence zone induced by mining is approximately 15 cm in front of the longwall face in the experimental scale (30 m in the prototype scale). These results are fairly consistent with the mining-induced pressure observed in the field tests (Shen et al., 2008; Gao et al., 2015).

4.2.3. Mining-induced pressure in fault-influenced zone

Fig. 8 also presents the distribution of mining-induced pressure at sensors Nos. 8–11 in fault-influenced zone. Comparing the sensors in uninfluenced and fault-influenced zones, it can be seen that the maximum value of mining-induced pressure in the fault-influenced zone is 26% larger than that in the uninfluenced zone. Taking sensor No. 11 for example, it is also indicated that the mining-induced pressure experiences a multi-stage during the coal seam mining, including slight increase, gradual increase, gradual decrease, sharp increase, succeeding stabilization, and sharp decrease (Fig. 10). The stages of slight and gradual increases are induced by the compaction of overlying strata before the roof collapse. The gradual stress decreases could appear due to the continuous roof caving. The alternative occurrence of fault stick and fault slip is the major reason for the stage of sharp increase and succeeding stabilization of mining-induced pressure. Finally, the mining-induced pressure decreases when the fault slip occurs. Since the sensor is still placed in the overlying strata and the large

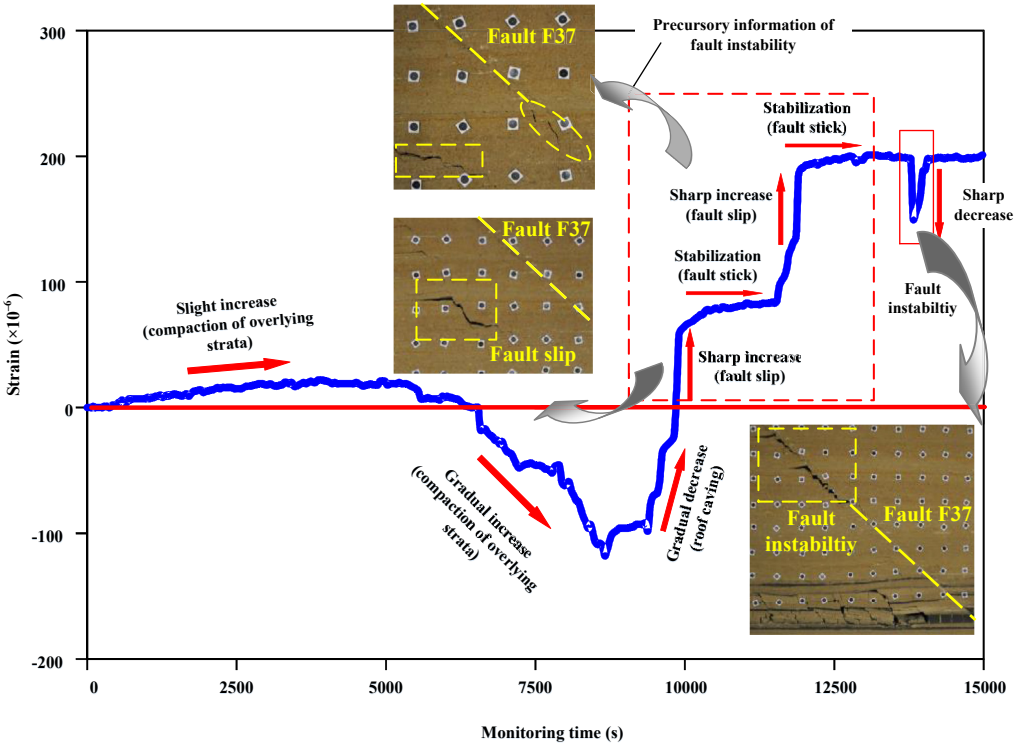

Fig. 10. Explanation of fault-slip process and precursors of fault slip.

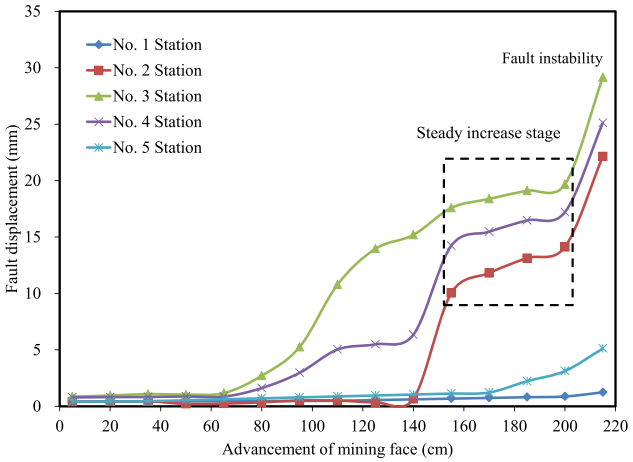

Fig. 11. Results of fault displacement obtained from monitoring stations around the fault F37.

area roof caving does not occur, the intense decrease does not appear when the fault slip occurs, which is the limitation of the present test.

In conclusion, the mining-induced pressure behaves violently in the fault-influenced zone, since the fault slip is a nonlinear dynamic process of steady accumulation and unsteady release of stress or even elastic strain energy. Therefore, the sharp increase and succeeding stabilization of stress could be identified as the precursory information of fault slip.

4.3. Characteristics of overlying strata deformation

To understand the precursory information of fault slip, the DIC technology is employed to detect the instant displacement of overlying strata near the fault F37. Fig. 11 presents the results of fault displacement obtained from five monitoring stations around the fault F37 (see Fig. 4a). It is suggested that the displacement obtained from the monitoring stations has a steady increase stage before the fault slip occurs. This stage could be recognized as the precursory information of fault slip as well. Fig. 12 shows the displacement contours of physical model before and after the fault slip. It should be noted that the displacement of roof strata increases sharply when the fault slip occurs.

5. Optimization of roadway support design and field verification

5.1. Optimization of roadway support design

As discussed in Section 2.2, it is assumed that the original support design will not be able to maintain the roadway stability under the influence of faults. The physical modeling results suggest that the pressure induced by the combined effect of mining activities and fault slip in the fault-influenced zone is greater than that in the uninfluenced zone. In addition, rock damage is serious in the fault-influenced zone, which could raise long-term safety concerns for the mine production.

As another main purpose of the cooperation between Zhengli coal mine and CUMTB, an effective support system to avoid excessive displacement or rapid failure of roadway in the fault-influenced zone is developed. Therefore, the support design is

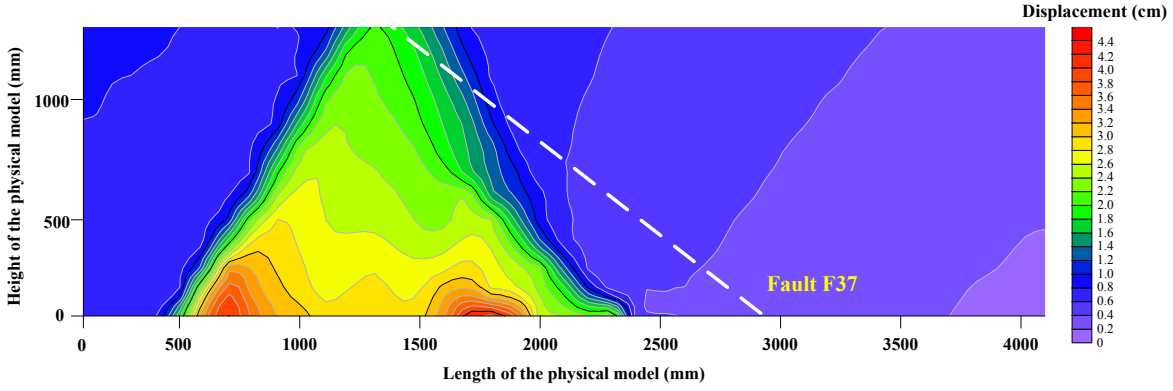

(a) Before the fault slip.

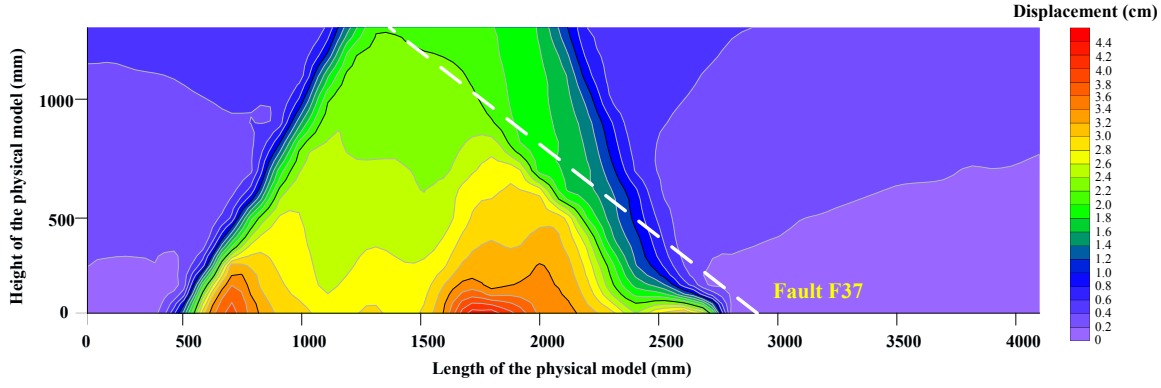

(b) After the fault slip.

Fig. 12. Displacement contours of physical model before and after fault slip.

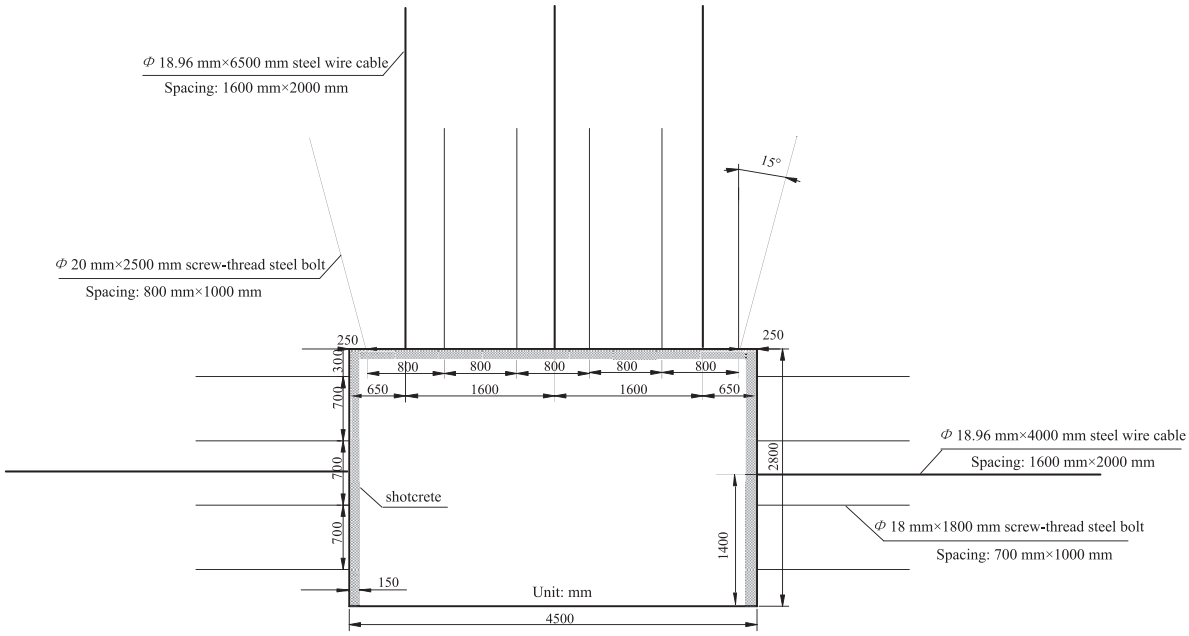

Fig. 13. Layout of optimized support design for haulage roadway in mining panel #14^{-1}103.

optimized with respect to the site-specific geological conditions of longwall panel #14^{-1}103 in the mining area #1. The support design of haulage roadway in the mining panel #14^{-1}103 is shown as an example.

According to the above results, the optimization strategy of roadway support focuses on enhancing the support resistance and utilizing the load bearing capacity of the stable surrounding rocks. Therefore, merely using 1.8 m long bolts in the ribs will not be able to maintain the roadway stability. Cables must be added to the support design for ribs. Meanwhile, to resist the roof collapse, three cables are used for the roof support. The modified support system is shown in Fig. 13. The optimized support design consists of bolts, cables and shotcrete combined with steel mesh and steel belt. The detailed support parameters are listed in Table 4.

The cables connect the combined arch structure formed by bolts to the stable surrounding rocks, thereby effectively mobilizing the load bearing capacity of the stable surrounding rocks. The installation of cables could increase the volume of stable strata participating in the support system.

In addition, shotcrete in the support system is used to keep the surrounding rock masses from being weathered, corroded and softened by groundwater. The field observations in the haulage roadway of the mining panel #14^{-1}103 indicate that the roadway is stable with the new designed support system.

5.2. Field verification

5.2.1. Arrangement of monitoring stations

As the mining panel #14^{-1}103 is influenced by faults F36 and F37, the haulage roadway in the mining panel #14^{-1}103 is selected in this study as a typical dynamic pressure area to verify the optimization of roadway support. The bolt and cable loads are monitored and investigated. The arrangement of monitoring stations in a cross-section of the roadway is shown in Fig. 14.

5.2.2. Field observation results

The monitoring results of bolt and cable loads under the optimized support design are shown in Fig. 15. It can be seen that although the bolt and cable loads continue to increase in the early installation period, the loads appear to be stable after 25 d during the observation. It is revealed that the cables play a significant role in utilizing the load bearing capacity of the stable surrounding rocks. The installation of cables could increase the volume of stable strata participating in the support system.

6. Conclusions

The physical modeling in presence of fault structure is employed to investigate the characteristics of overlying strata collapse and

Table 4
Detailed support parameters of haulage roadway in mining panel #14^{-1}103.

Support type	Specification (mm × mm)	Material	Elongation (%)	Array spacing (mm)	Spacing in cross-section (mm)	Pretension force (kN)
Bolt in the roof	ϕ20 × 2500	High-strength screw-thread steel	18	1000	800	≥50
Bolt in the ribs	ϕ18 × 1800	High-strength screw-thread steel	18	1000	700	≥50
Cable in the roof	ϕ18.96 × 6500	Q235 Steel wire	7	2000 (2-1-2 in row)	1600	≥30
Cable in the ribs	ϕ18.96 × 4000	Q235 Steel wire	7	2000 (1-0-1 in row)	1600	≥30
Shotcrete	Thickness is 50–150 mm to keep the rock from being weathered					

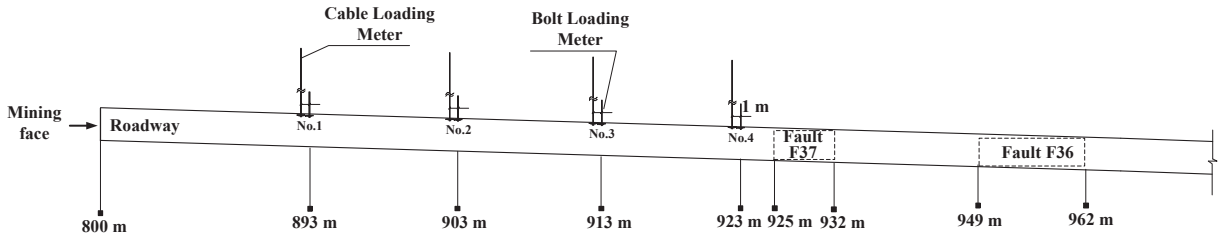

Fig. 14. Arrangement of filed observation stations in the haulage roadway in mining panel #14^{-1}103.

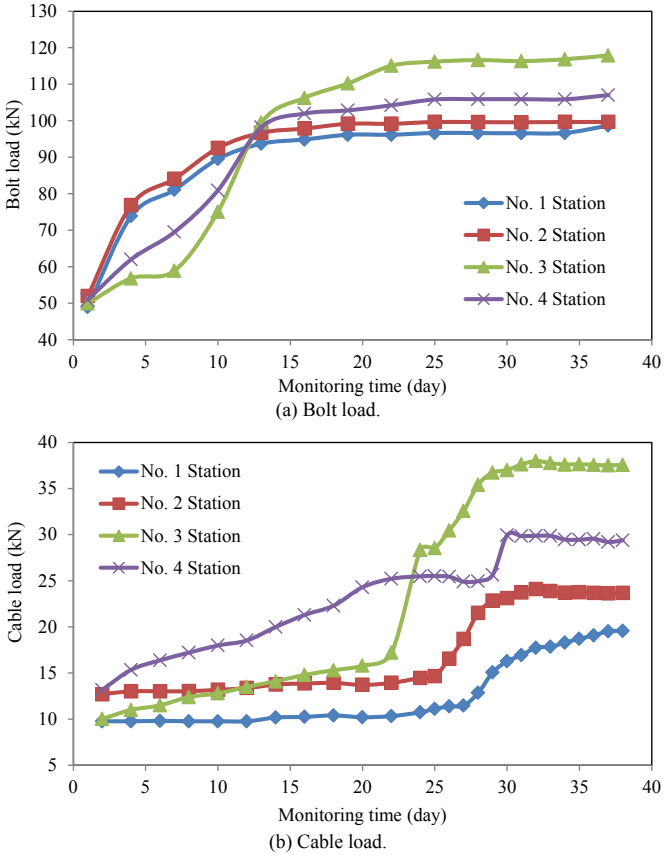

Fig. 15. Field observation results of bolt and cable loads.

mining-induced pressure in the uninfluenced and fault-influenced zones. The main conclusions drawn from the investigations are summarized below:

(1) The presence of faults and other adverse geological condition could seriously cause the expansion of the rock damage and dynamic accidents in the underground mining. The mining-induced pressure and the extent of damaged rock mass in the fault-influenced zone are greater than those in the uninfluenced zone due to the combined effect of mining activities and fault slip.
(2) The sharp increase and the succeeding stabilization of stress or steady increase in displacement could be identified as the precursory information of fault slip.
(3) Considering the large mining-induced pressure in the fault-influenced zone, a new support design utilizing cables is developed. It is confirmed that the roadway is maintained in a good condition by the new system.

Conflict of interest

We wish to confirm that there are no known conflicts of interest associated with this publication and there has been no significant financial support for this work that could have influenced its outcome.

Acknowledgment

This research is financially supported by the National Natural Science Foundation of China (No. 41502184), Beijing Natural Science Foundation (No. 2164067), National Key Research and Development Program (No. 2016YFC0801401), Fundamental Research Funds for the Central Universities (No. 2014QL01), and Innovation Training Programs for Undergraduate Students (Nos. 201411413054 and SKLCRSM14CXJH08). The authors would like to thank the reviewers and editors who presented critical and constructive comments for the improvement of this paper. The authors wish to express their gratitude to Dr. Qingdong Qu and Dr. Yucang Wang from CSIRO for their works to improve the English of this paper.

References

Bryant WA. Fault. In: Encyclopedia of natural hazards. Dordrecht, Netherlands: Springer; 2013. p. 317–20.
Cai W, Dou LM, Cao AY, Gong SY, Li ZL. Application of seismic velocity tomography in underground coal mines: a case study of Yima mining area, Henan, China. Journal of Applied Geophysics 2014;109:140–9.
Castro LAM, Carter TG, Lightfoot N. Investigating factors influencing fault-slip in seismically active structures. In: Proceedings of the 3rd CANUS Rock Mechanics Symposium, Toronto; 2009. p. 1–12.
Cook NGW. The application of seismic techniques to problems in rock mechanics. International Journal of Rock Mechanics and Mining Sciences & Geomechanics Abstracts 1964;1(2):169–79.
Dou LM, Chen TJ, Gong SY, He H, Zhang SB. Rockburst hazard determination by using computed tomography technology in deep workface. Safety Science 2012;50(4):736–40.
Du WF, Peng SP, Shi SZ. Seismic interpretation of deep buried structure characteristics and its influence on coal mine safety. Journal of China Coal Society 2015;40(3):640–5 (in Chinese).
Fuenkajorn K, Phueakphum D. Physical model simulation of shallow openings in jointed rock mass under static and cyclic loadings. Engineering Geology 2010;113(1–4):81–9.
Gao FQ, Stead D, Kang HP. Numerical simulation of squeezing failure in a coal mine roadway due to mining-induced stresses. Rock Mechanics and Rock Engineering 2015;48(4):1635–45.
Ghabraie B, Ren G, Zhang XY, Smith J. Physical modeling of subsidence from sequential extraction of partially overlapping longwall panels and study of substrata movement characteristics. International Journal of Coal Geology 2015;140:71–83.
Gochioco LM, Cotten SA. Locating faults in underground coal mines using high-resolution seismic reflection techniques. Geophysics 1989;54(12):1521–7.
Goyal M, Kumar S, Singh TN. Study of sub-level caving method of thick seam mining by equivalent material modeling technique. Indian Journal of Engineers 1997;5:33–45.
Hlousek F, Hellwig O, Buske S. Geothermal reservoir characterization in crystalline rock using 3D seismics (Schneeberg, Germany). In: Proceedings of the World Geothermal Congress, Melbourne, Australia; 2015. p. 1–8.
Jain A, Verma AK, Vishal V, Singh TN. Numerical simulation of fault reactivation phenomenon. Arabian Journal of Geosciences 2013;6(9):3293–302.

Jiang FX, Qu XC, Yu ZX, Wang CW. Real-time monitoring and measuring early-warning technology and development of mine pressure bumping. Coal Science and Technology 2011;39:59–64 (in Chinese).
Jiang YD, Wang T, Zhao YX, Wang WJ. Experimental study of the mechanisms of fault reactivation and coal bumps induced by mining. Journal of Coal Science and Engineering 2013;19(4):507–13.
Jiang YD. Fundamental research on mechanism and prevention of coal mine dynamic disasters at great depth. National Basic Research Program Report, No. 2010CB226800. Beijing: China University of Mining & Technology; 2014 (in Chinese).
Jiang YD, Pan YS, Jiang FX, Dou LM, Ju Y. State of the art review on mechanism and prevention of coal bumps in China. Journal of China Coal Society 2014;39(2):205–13 (in Chinese).
Kecojevic V, Willis D, Wilkinson W, Schissler A. Computer mapping of faults in coal mining. International Journal of Coal Geology 2005;64(1–2):79–84.
Kozicki J, Tejchman J. Experimental investigations of strain localization in concrete using digital image correlation (DIC) technique. Archives of Hydroengineering and Environmental Mechanics 2007;54(1):3–24.
Li HC. Similar simulation experiment of mine pressure. Xuzhou: China University of Mining & Technology Press; 1988 (in Chinese).
Li JC, Ma GW, Zhao J. Analysis of stochastic seismic wave interaction with a slippery rock fault. Rock Mechanics and Rock Engineering 2011;44(1):85–92.
Li ZL, Dou LM, Cai W, Wang GF, He J, Gong SY, Ding YL. Investigation and analysis of the rockburst mechanism induced within fault-pillars. International Journal of Rock Mechanics and Mining Sciences 2014;70:192–200.
Lin Q, Labuz JF, Cattaneo S. Digital image correlation and the fracture process in rock. In: Proceedings of the 44th US Rock Mechanics Symposium and 5th U.S.-Canada Rock Mechanics Symposium, Salt Lake City, UT; 2010.
Liu J, Feng XT, Ding XL, Zhang J, Yue DM. Stability assessment of the Three-Gorges Dam foundation, China, using physical and numerical modeling—Part I: physical model tests. International Journal of Rock Mechanics and Mining Sciences 2003;40(5):609–31.
Liu JH, Zhai MH, Guo XS, Jiang FX, Sun GJ, Zhang ZW. Theory of coal burst monitoring using technology of vibration field combined with stress field and its application. Journal of China Coal Society 2014;39(2):353–63 (in Chinese).
Mao LT, Hao N, An LQ, Chiang FP, Liu HB. 3D mapping of carbon dioxide-induced strain in coal using digital volumetric speckle photography technique and X-ray computer tomography. International Journal of Coal Geology 2015;147–148:115–25.
Mao LT, Zhu XX, An LQ, Cai GS, Hao N. Application of digital target marker image correlation method in model experiment. Journal of Liaoning Technical University: Natural Science 2013;32(10):1367–73 (in Chinese).
McKinnon SD. Triggering of seismicity remote from active mining excavations. Rock Mechanics and Rock Engineering 2006;39(3):255–79.
Monjezi M, Singh TN. Slope instability in an opencast mine. Coal International 2000;5:145–7.
Orlic B, Wassing BBT. A study of stress change and fault slip in producing gas reservoirs overlain by elastic and viscoelastic caprocks. Rock Mechanics and Rock Engineering 2013;46(3):421–35.
Ortlepp WD. Observation of mining-induced faults in an intact rock mass at depth. International Journal of Rock Mechanics and Mining Sciences 2002;37(1):423–36.
Peng SP, Du WF, Zhao W, Shi SZ, He DK. 3D coalfield seismic integrated interpretation technique in complex geological condition. Chinese Journal of Rock Mechanics and Engineering 2008;27(Suppl. 1):2760–5 (in Chinese).
Sainoki A, Mitri HS. Dynamic behavior of mining-induced fault slip. International Journal of Rock Mechanics and Mining Sciences 2014a;66:19–29.
Sainoki A, Mitri HS. Dynamic modeling of fault-slip with Barton's shear strength model. International Journal of Rock Mechanics and Mining Sciences 2014b;67:155–63.
Sainoki A, Mitri HS. Effect of slip-weakening distance on selected seismic source parameters of mining-induced fault-slip. International Journal of Rock Mechanics and Mining Sciences 2015;73:115–22.
Scheidhauer M, Marillier F, Thierry P. Detailed 3D seismic imaging of a fault zone beneath Lake Geneva, Switzerland. Basin Research 2005;17(1):155–69.
Shen B, King A, Guo H. Displacement, stress and seismicity in roadway roofs during mining-induced failure. International Journal of Rock Mechanics and Mining Sciences 2008;45(5):672–88.
Singh AK, Kainthola A, Singh TN. Prediction of factor of safety of a slope with an advanced friction model. International Journal of Rock Mechanics and Mining Sciences 2012;55:164–7.
Singh PK, Singh TN, Singh DP. A study of the effect of fault plane on slope stability of opencast mine by equivalent material-modeling. MineTech 1998:37–44.
Singh TN, Singh DP. Slope behavior in an opencast mine over old underground voids. International Journal of Surface Mining 1991;4(5):195–201.
Singh TN, Singh DP. Prediction of instability of slopes in an opencast mine over old surface and underground workings. International Journal of Surface Mining 1992a;6(2):81–9.
Singh TN, Singh DP. Assessing stability of voids in a multi-seam opencast mining block. International Journal of Colliery Guardian 1992b;240(4):159–64.
Tripathy A, Singh TN. Physical and numerical simulation of instability of slope. In: National Conference on Advanced Trends in Civil Engineering and Sustainable Development, Mangalore, India; 2016.
Vishal V, Das R, Singh TN. Investigating the frictional response of granitic rock surface: an experimental approach. Journal of the Geological Society of India 2012;80(4):493–8.
Wallace RE, Morris HT. Characteristics of faults and shear zones in deep mines. Pure and Applied Geophysics 1986;124:107–25.
Wang HW, Jiang YD, Xue S, Shen BT, Wang C, Lu JG, Yang T. Assessment of excavation damaged zone around roadways under dynamic pressure induced by an active mining process. International Journal of Rock Mechanics and Mining Sciences 2015;77:265–77.
Zhu WS, Li Y, Li SC, Wang SG, Zhang QB. Quasi-three-dimensional physical model tests on a cavern complex under high in-situ stresses. International Journal of Rock Mechanics and Mining Sciences 2011;48(2):199–209.

Hongwei Wang obtained a M.Sc. and a Ph.D. degree from China University of Mining and Technology, Beijing. He is associate professor of engineering mechanics at the School of Mechanics and Civil Engineering, China University of Mining & Technology, Beijing. He is a member of the Chinese Society for Rock Mechanics and Engineering, Chinese Society of Theoretical and Applied Mechanics, and China Coal Society. He is the author or co-author of more than 30 scientific papers which focus on the mechanism of coal bumps, roadway support and characteristics of tectonic movement. In 2014, he won the excellent dissertation award by the Chinese Society for Rock Mechanics and Engineering. In recent years, he has been financially supported by the National Natural Science Foundation of China, Beijing Natural Science Foundation and Major State Basic Research Development Program.